



Dalton
Transactions

Design and Synthesis of Photoluminescent Active Interpenetrating Metal–Organic Frameworks using N-2-Aryl-1,2,3-Triazole Ligands

Journal:	<i>Dalton Transactions</i>
Manuscript ID	DT-COM-03-2020-000933.R2
Article Type:	Communication
Date Submitted by the Author:	06-Apr-2020
Complete List of Authors:	Shi, Xiaodong; University of South Florida, Chemistry Li, Jingyang; Jilin University He, Ying; University of South Florida, Chemistry Wang, Li; Jilin University College of Chemistry, Pan, Qin He; Hainan University, Materials and Chemical Engineering Song, Zhiguang; Jilin University, college of chemistry

SCHOLARONE™
Manuscripts

COMMUNICATION

Design and Synthesis of Photoluminescent Active Interpenetrating Metal–Organic Frameworks Using N-2-Aryl-1,2,3-Triazole Ligands

 Jingyang Li^a, Ying He^b, Li Wang^a, Qinhe Pan^c, Zhiguang Song^{*a} and Xiaodong Shi^{*b}

 Received 00th January 20xx,
 Accepted 00th January 20xx

DOI: 10.1039/x0xx00000x

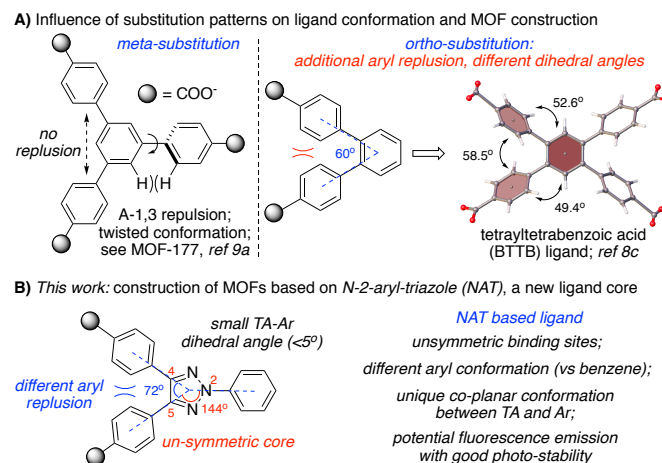
www.rsc.org/

N-2-aryl-1,2,3-triazole derivatives were synthesized as a new ligand system for the construction of photoluminescent active metal-organic frameworks (MOFs). Crystal structures revealed that the five-membered triazoles give unsymmetrical conformation with the two C4,C5-substituted benzenes adopted “twisted-plane” geometry. As the result, a MOF constructed from this ligand exhibited cross-layer interactions with improved water stability (at 100 °C for 24 hours). Furthermore, enhanced photoluminescence emissions were observed upon the formation of MOF structures (Φ up to 30%), suggesting potential applications of this photoactive porous material through this new ligand design.

The past two decades have evidenced the fast growing of porous material research.¹ With the large surface area, tunable pore sizes, diverse geometries and accessible functional sites, porous materials have shown superior applications in various research fields, including gas molecule storage, chemical catalysis and molecular sensing.² As a very important area of porous materials, metal-organic frameworks (MOFs) have gained increasing attention in current chemical and material research.³ Although many well-developed molecular scaffolds with well-defined geometry have been reported in the past two decades, new building blocks with alternative binding patterns are always welcome and desirable since they could offer new coordination mode with potential interesting functionality.⁴ Herein, we report N-2-aryl-1,2,3-triazole derivatives as linkers for the construction of metal-organic frameworks with significantly improved water stability, enhanced luminescence emission and selective CO₂ adsorption.

Over the past decade, our group has been working on the development of 1,2,3-triazoles as building blocks for important

chemical, material and biological applications.⁵ With the success in discovering several new synthetic methods for effective preparation of 1,2,3-triazole derivatives, our group first reported the strong fluorescence emission associated with N-2-aryl-1,2,3-triazoles (NATs).⁶ Moreover, X-ray crystal structures revealed co-planar conformation between triazole and N-2-aryl rings, which could account for the observed strong photo emission.⁷ With the continued interest in developing new chemical platforms for material and biological research, we put our attention into the potential applications of this new molecular scaffold into porous material constructions. In this manuscript, we report the first two MOF structures recently obtained from ligands based on the NAT core, **NAT-MOF-1** and **NAT-MOF-2**.



Scheme 1. NAT as the core structure for MOF construction

As shown in Scheme 1A, multi-carboxylate ligands have been widely used for MOF construction through the COO⁻ coordination with various metal cations.⁸ For example, the 1,3,5-triaryl-benzic acid ligand has been used for the preparation of MOF-177.⁹ Certainly, ligand conformation will greatly influence the overall binding pattern and final MOF topology.¹⁰ For benzene-based ligands, two general conformation concerns are A)

^a State key Laboratory of Supramolecular Structure and Materials, College of Chemistry, Jilin University, Changchun, Jilin 13002 China; E-mail szg@jlu.edu.cn

^b Department of Chemistry, University of South Florida, 4202 E. Fowler Avenue, Tampa, Florida 33620, United States. E-mail: xmshi@usf.edu

^c Key Laboratory of Advanced Materials of Tropical Island Resources Hainan University, Haikou 570228, P. R. China.

^d †Electronic Supplementary Information (ESI) available. See DOI: 10.1039/x0xx00000x

binding angle between coordination sites and B) dihedral angle between the two adjacent aryl groups.¹¹ For bis-benzene system, twisted conformation is observed in almost all cases due to the strong A-1,3 repulsion between the two benzene rings.¹² Interestingly, although some examples have been reported in the literature, MOFs from ligands with 1,2-substituted benzene structures are much less compared with the 1,3-substituted analogues.¹³ This is likely due to the smaller coordination angle (60° for 1,2-subst vs 120° for 1,3-subst), which may cause the increased steric hindrance toward metal cation coordination.¹⁴

Comparing with popular benzene-core ligands, the NAT ligand has very different conformation in both perspectives. First, the two C4, C5-substituted groups give a bigger binding angle (72°), which might lead to preferred aryl group conformation with different overall repulsion. Meanwhile, the triazole ring and N-2 aryl ring adopted co-planar conformation by avoiding the A-1,3 repulsion. More importantly, while N-1-aryl triazole gave almost no fluorescence emission, many N-2-aryl derivatives are good fluorophore, giving strong emission in UV/blue light region.¹⁵ All these unique structural features initiated our interest to explore whether NAT can be used as ligands for MOF preparation with interesting new functions. To the best of our knowledge, there are few triazole based MOF structures reported so far and no NAT based MOF has ever been reported.¹⁶ This is likely due to the challenges associated with synthesis of ligands and challenging structural control.¹⁷ With the recent success in triazole synthesis and functionalization, we prepared two NAT based ligands, **L1** and **L2** (Figure 1A) and applied them for MOF constructions under various metal binding conditions.

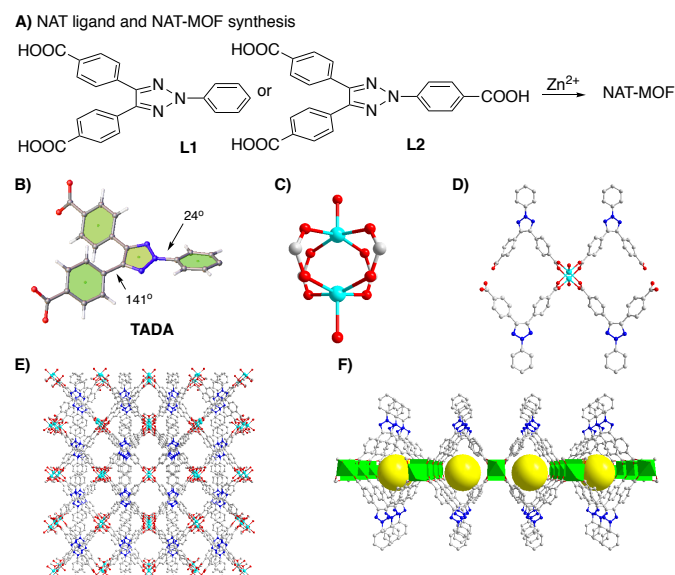


Figure 1. NAT-MOF synthesis and crystal structure of **NAT-MOF-1**: A) ligand and the general MOF synthetic route; B) NAT ligand **L1** (TADA); C) Zn paddle-wheel SBU; D) Connectivity between TADA and paddle-wheel SBU; E) View of **NAT-MOF-1** along c axes; F) View of a fragment of **NAT-MOF-1** along c axes showing fitted pores.

Using ligand **L1**, (4,4'-(2-phenyl-1,2,3-triazole-4,5-diyl)dibenzoic acid (TADA), with no carboxylate on the N2-phenyl group on triazole (Figure 1B), **NAT-MOF-1** was obtained through solvothermal conditions by dissolving $\text{Zn}(\text{NO}_3)_2 \cdot 6\text{H}_2\text{O}$

and **L1** (2:1) in solvents (1:1 DMF:MeOH) and heated at 85 °C for 72 hours. The FT-IR spectra (Figure S2a) of resulting MOF revealed the disappearance of carboxylic acid groups around 2998 cm^{-1} and the symmetric and asymmetric stretching of carboxylate groups at 1414 cm^{-1} and 1529 cm^{-1} . Fortunately, a crystal was successfully grown with structure revealed a di-nuclear paddle-wheel secondary building unit (SBU) that two Zn atoms are binding to four **L1** in approximately 90° with two dimethyl ether molecules coordinated on the top (Figure 1C). Packing of unit cell along the c axes and a fragment of **NAT-MOF-1** along c axes showing fitted pores are also revealed in Figure 1E and Figure 1F respectively.

Treating NAT ligand **L2**, 4,4',4''-(2H-1,2,3-triazole-2,4,5-triyl)tribenzoic acid (TATA), under similar solvothermal conditions gave **NAT-MOF-2**. The FT-IR spectra showed the characteristic band of coordinated carboxylate groups at 1377 and 1606 cm^{-1} (Figure S2b). The broad band at 2991 cm^{-1} for carboxylic acid stretching disappeared, indicating the binding with metal cations. The crystal structure of **NAT-MOF-2** was also successfully obtained as shown in Figure 2.

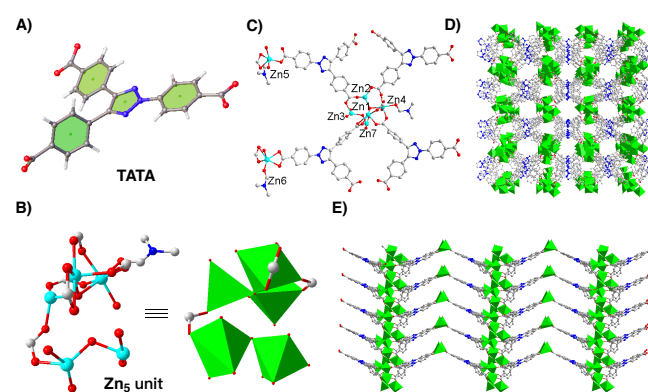


Figure 2. Crystal structure and structural components of **NAT-MOF-2**: A) triazole based linker **L2**; B) Center coordination environments of Zn_5 unit; C) Overall coordination environments between ligand TATA and $\text{Zn}(\text{II})$ ions; D) View of **NAT-MOF-2** along c and E) b axes respectively.

The crystal structure of **NAT-MOF-2** demonstrated a highly interpenetrated framework. Each repeating unit is composed of seven Zn (II) ions and four NAT ligands **L2** (Figure 2B, 2C). Zinc ions including Zn1, Zn2, Zn3, Zn4 and Zn7 compose a Zn_5 unit while the vertices of the network are connected by Zn5 and Zn6 in the horizontal direction and Zn3 and Zn7 connect the interlayers with C5-substituted carboxylate group to give structure extension along vertical directions, affording the interpenetrated networks. Interestingly, with the highly unsymmetrical NAT core, the overall **NAT-MOF-2** structure resembles a “roof tile” alignment. As shown in the crystal structure, this tile-like interpenetrated network is formed with the penetration of both horizontal and vertical directions. The stacking of tiles was assembled through the formation of the Zn_5 unit locating in the middle of the tile. Meanwhile, due to highly unsymmetrical factor of the crystal structure and unsymmetrical Zn_5 unit coordination environments along the vertical direction in the center, there are four different conformations of **L2** from the repeating units. To be specific, dihedral angles between NAT and carboxylate groups and the binding angles (107°-164°) of carboxylates from N-2 and C-4 position resembled the basic layer of the tile structure appear unique in general. Interestingly, the binding

modes for these two NAT-MOFs are dramatically different, which highlighted the importance of conformation control of this newly developed unsymmetrical NAT ligands. Powder X-ray diffraction (PXRD) spectra of both NAT-MOFs were collected. The diffraction patterns of the tested samples and the calculated data from crystal structure were compared. (Figure S1) With the structures of both NAT-MOFs confirmed by X-ray, we set out to explore the influence of different topologies towards the resulting MOF material functions.

Unlike typical di-aryl compounds, one unique property of NAT ligand is the co-planar conformation between triazole and N-2 aryl rings. Our group has previously demonstrated that N-2-aryl triazoles could exhibit strong fluorescence while the N-1 isomer gives almost no emission. As a new class of small molecule organic fluorophore, NAT has some unique advantages, including luminescence efficiency, high thermal stability, good accessibility and easy modification.¹⁸ However, during our previous studies, the emission efficiency was significantly reduced when introducing carboxylate group on N-2-aryl position. This is likely due to the various relaxation pathways (*i.e.* vibrational and rotational) typically associated with carboxylate groups, which quenched the photo-excitation state. Considering that carboxylate will hold more locked conformation in MOF complexes over free ligand, one could rationalize that improved fluorescence emission might be achieved upon MOF formation. To verify this hypothesis, the solid-state photoluminescence emission of both ligands and MOFs were measured. As expected, dramatic increase of fluorescence intensity was obtained in both NAT-MOFs over non-coordinated ligands (Figure 3).

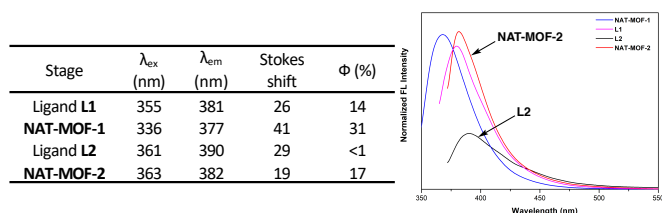


Figure 3. Enhanced fluorescence emission upon formation of NAT-MOFs

First, comparing with non-substituted NAT compounds, the carboxylate group caused the reduction of photoemission, especially on the N-2-aryl position. While N-2-phenyl ligand L1 (TADA) still gives luminescence emission in solid state with reduced quantum yield (Φ) as 13.8%, dramatic quenching effect was observed with the N-2-benzoylic acid ligand L2 (TATA, $\Phi=0.59\%$). This is consistent with our previous report that the actual fluorophore in NAT is the N-2-aryl moiety. Upon formation of MOF structures, a significantly increase of emission intensity was obtained for both NAT-MOF-1 ($\Phi=30.8\%$) and NAT-MOF-2 ($\Phi=17.5\%$). This emission enhancement could be attributed to Zn-O coordination, which significantly reduced the possibility of excitation state relaxation, along with plausible π - π stacking between adjacent aromatic moieties. This result is exciting since it suggested the strong potential of this new MOF materials for photoactivation related applications.

Comparing with benzene-based ligands, another interesting feature of the triazole-based ligand is the bigger coordination angle between substituted groups at C4 and C5 position (*vs* 1,2-substituted benzene). Clearly, this different binding angles will influence MOF topology as seen in the X-ray crystal structures.

Stability of MOFs in water plays a crucial role for potential

application of porous materials in aqueous environment.¹⁹ Generally, water stability depends on steric effects of the ligand and strength of metal–ligand coordination.²⁰ Therefore, solvent and moisture stability were also tested with this new type NAT-MOF by comparing the PXRD data of MOF samples upon soaking in a variety of solvents, including MeOH, Acetonitrile, DCM and water. Although NAT-MOF-1 showed poor stability in organic solution, it demonstrated relatively good stability in aqueous solution. As shown in Figure 4, even after being immersed in boiling water for 24 hours, NAT-MOF-1 maintained most of its crystalline frameworks with several changes of diffraction angle signals. In contrast, NAT-MOF-2 presented a complete destructive breakdown of porous frameworks as almost no signals observed in the PXRD spectra.

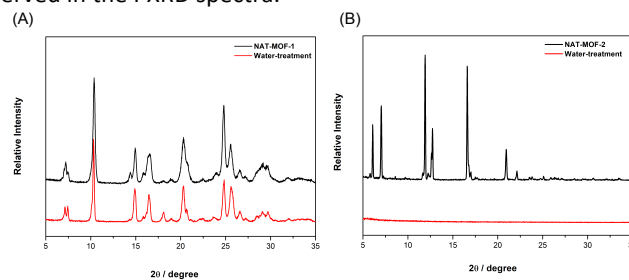


Figure 4. NAT-MOF-1 and NAT-MOF-2 water stability evaluated by PXRD patterns

As porous materials, the gas sorption capacity and selectivity are certainly important factors to be evaluated. The CO₂ adsorption data were collected at 195 K to examine the porosity of these NAT-MOFs (Figure 5A).

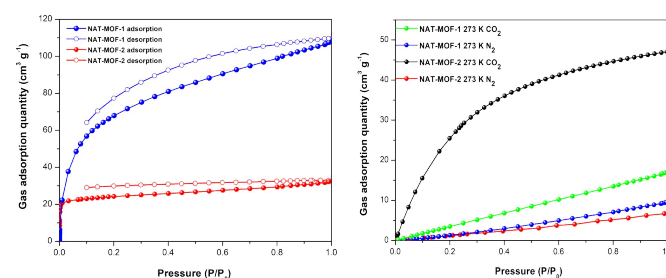


Figure 5. (A) CO₂ sorption of NAT-MOF-1 and NAT-MOF-2 at 195 K (B) CO₂ and N₂ sorption isotherm of NAT-MOF-1 and NAT-MOF-2 at 273 K

Both frameworks behave reversible type-I isotherm adsorption features, in which gas molecules present sharp adsorption at relatively low pressure ($P/P_0 < 0.1$) and reach to plateau subsequently. Desorption hysteresis loop happened on both frameworks, which could be ascribed to the existence of mesopores and inevitable interaction between N atoms from 1,2,3-triazole backbones and oxygen from CO₂ molecules. The Brunauer-Emmett-Teller (BET) and Langmuir surface area were calculated to be 216 m² g⁻¹ and 313 m² g⁻¹ for NAT-MOF-1 and 69 m² g⁻¹ and 96 m² g⁻¹ for NAT-MOF-2. NAT-MOF-1 showed higher BET surface areas over NAT-MOF-2 likely due to the size of micropores caused by higher dV/dw and highly symmetric structures. As the result, NAT-MOF-1 gave the maximum N₂ uptake of 9.5 cm³ g⁻¹, which is higher than the N₂ uptake of 6.7 cm³ g⁻¹ for NAT-MOF-2 at 273 K (Figure 5B). The total pore volumes of 0.12 cm³ g⁻¹ (NAT-MOF-2) and 0.52 cm³ g⁻¹ (NAT-MOF-1) were estimated from the Horvath-Kawazoe calculation (Figure S4).

Notably, carbon dioxide (CO₂) capture and storage (CCS) is

of importance for the environmental concern with growing atmospheric CO₂ emissions caused by use of fossil fuels.²¹ To evaluate CO₂ uptake performances of these new MOFs, CO₂ adsorption isotherms were collected on the activated samples at 273 K, as shown in Figure 5(B). The results revealed 17 cm³ g⁻¹ and 47 cm³ g⁻¹ maximum adsorption of CO₂ at 273 K for **NAT-MOF-1** and **NAT-MOF-2** respectively. The value of CO₂/N₂ selectivity was obtained by Ideal solution adsorbed theory (IAST) with a good correlation factor ($R^2 > 0.999$). In general, nitrogen atoms in the organic linker and the π -stacking could increase the CO₂ adsorption capacity.²² Although the CO₂ adsorption selectivity was modest (4.8, Figure S5), the fact that CO₂ can be selected adopted in this simple framework highlighted the polarized pore nature associated with the unique 1,2,3-triazole building blocks for CO₂ adsorption. In addition, the higher adsorption of **NAT-MOF-2** compared to **NAT-MOF-1** is presumably due to the extra carboxylate in **L2** which result in more dipole-dipole interactions despite of the interpenetrating framework. It is expected that further modification of this simple and easy-access structure could be done with improved adsorption ability and selectivity.

In conclusion, we reported herein is the investigations of N-2-aryl-1,2,3-triazole derivatives as ligands for the construction of MOF materials. Comparing with widely applied benzene-based linkers, the NAT offers several unique features, including the excellent fluorescence emission, co-planar conformation and larger binding angle at C4 and C5 position. Two new metal-organic frameworks (NAT-MOFs) were successfully obtained upon coordination with Zn and their structures have been fully characterized by single crystal X-ray and PXRD. Some interesting properties have been revealed with these NAT-MOFs, including dramatically enhanced photo luminance emission and selective CO₂ adsorption. Overall, these studies not only set up a solid foundation for the design principle for the development of new porous materials using NAT core, but also demonstrates the possibility to construct new functional NAT-MOFs with good photoactivity. These studies are currently undergoing in our lab and will be reported in due course.

Conflicts of interest

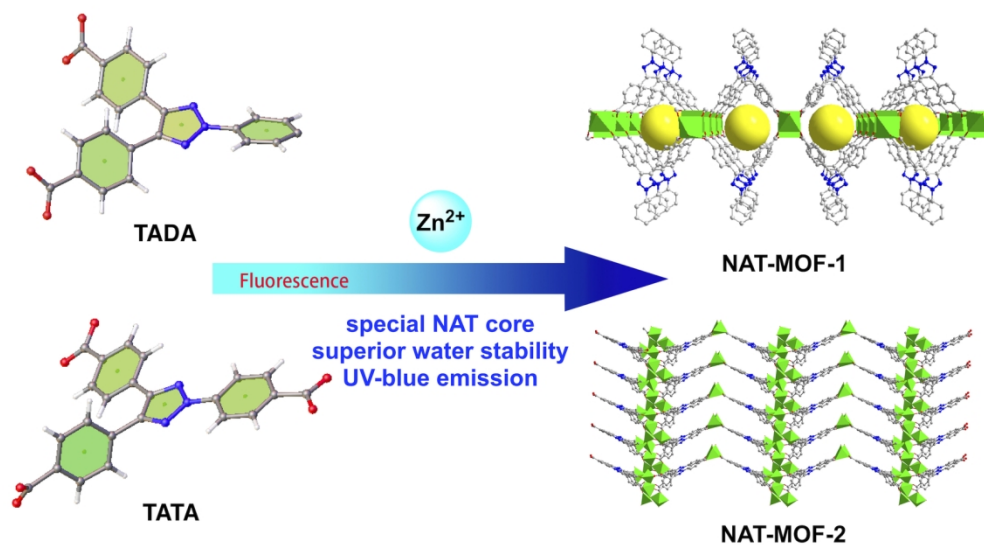
There are no conflicts to declare.

Acknowledgements

We are grateful to NSF (CHE-1665122), Jilin Province (20170307024YY, 20190201080JC) for financial support.

Notes and references

- (a) O. M. Yaghi, M. O'Keeffe, N. W. Ockwig, H. K. Chae, M. Eddaoudi and J. Kim, *Nature*, 2003, **423**, 705-714; (b) M. E. Davis, *Nature*, 2002, **417**, 813-821.
- (a) R. B. Getman, Y. S. Bae, C. E. Wilmer and R. Q. Snurr, *Chem. Rev.*, 2012, **112**, 703-723; (b) H. Zhou, J. R. Long and O. M. Yaghi, *Chem. Rev.*, 2012, **112**, 673-674. (c) Y. Zhao, S. Qi, Z. Niu, Y. Peng, C. Shan, G. Verma, L. Wojtas, Z. Zhang, B. Zhang, Y. Feng, Y. Chen and S. Ma, *J. Am. Chem. Soc.*, 2019, **141**, 14443-14450.
- D. Feng, W. Chung, Z. Wei, Z. Gu, H. Jiang, Y. Chen, D. J. Darensbourg and H. Zhou, *J. Am. Chem. Soc.*, 2013, **135**, 17105-17110.
- M. Eddaoudi, J. Kim, N. Rosi, D. Vodak, J. Wachter, M. O'Keeffe and O. M. Yaghi, *Science*, 2002, **295**, 469-472.
- (a) R. Cai, X. Ye, Q. Sun, Q. He, Y. He, S. Ma and X. Shi, *ACS Cat.*, 2017, **7**, 1087-1092; (b) X. Ye, C. Xu, L. Wojtas, N. Akhmedov, H. Chen and X. Shi, *Org. Lett.*, 2016, **18**, 2970-2973.
- (a) Y. Zhang, X. Ye, J. L. Petersen, M. Li and X. Shi, *J. Org. Chem.*, 2015, **80**, 3664-3669; (b) D. Wang, X. Ye and X. Shi, *Org. Lett.*, 2010, **12**, 2088-2091.
- Y. Liu, W. Yan, Y. Chen, J. L. Petersen and X. Shi, *Org. Lett.*, 2008, **10**, 5389-5392.
- (a) T. He, Y. Zhang, H. Wu, X. Kong, X. Liu, L. Xie, Y. Dou and J. Li, *ChemPhysChem*, 2017, **18**, 3245-3252; (b) B. Gómez-Lor, E. Gutiérrez-Puebla, M. Iglesias, M. A. Monge, C. Ruiz-Valero, and N. Snejko, *Chem. Mater.*, 2005, **17**, 2568-2573; (c) J. R. Karra, Y. Huang and K. S. Walton, *Cryst. Growth Des.*, 2013, **13**, 1075-1081.
- (a) H. K. Chae, D. Y. Siberio-Pérez, J. Kim, Y. Go, M. Eddaoudi, A. J. Matzger, M. O'Keeffe and O. M. Yaghi, *Nature*, 2004, **427**, 523-527; (b) Y. Zhang, H. Furukawa, N. Ko, W. Nie, H. Park, S. Okajima, K. E. Cordova, H. Deng, J. Kim and O. M. Yaghi, *J. Am. Chem. Soc.*, 2015, **137**, 2641-2650.
- D. Zhao, D. J. Timmons, D. Yuan and H. Zhou, *Acc. Chem. Res.*, 2011, **44**, 123-133.
- (a) F. Lundvall, P. D. C. Dietzel and H. Fjellvag, *Acta Cryst.*, 2016, **72**, 328-330; (b) M. E. Braun, C. D. Steffek, J. Kim, P. G. Ras-mussen and O. M. Yaghi, *Chem. Commun.*, 2001, 2532-2533.
- D. Bara, C. Wilson, M. Mörtel, M. M. Khusniyarov, S. Ling, B. Slater, S. Sproules and R. S. Forgan, *J. Am. Chem. Soc.*, 2019, **141**, 8346-8357.
- B. Li, H. Wen, Y. Cui, W. Zhou, G. Qian and B. Chen, *Adv. Mater.*, 2016, **28**, 8819-8860.
- (a) J. Pang, S. Yuan, J. Qin, C. Liu, C. Lollar, M. Wu, D. Yuan, H. Zhou and M. Hong, *J. Am. Chem. Soc.*, 2017, **139**, 16939-16945; (b) Y. Wang, L. Feng, W. Fan, K. Wang, X. Wang, X. Wang, K. Zhang, X. Zhang, F. Dai, D. Sun and H. Zhou, *J. Am. Chem. Soc.*, 2019, **141**, 6967-6975.; (b) Y. Wang, L. Feng, W. Fan, K. Wang, X. Wang, X. Wang, K. Zhang, X. Zhang, F. Dai, D. Sun and H. Zhou, *J. Am. Chem. Soc.*, 2019, **141**, 6967-6975.
- (a) Q. Lai, Q. Liu, K. Zhao, C. Shan, L. Wojtas, Q. Zheng, X. Shi and Z. Song, *Chem. Commun.*, 2019, **55**, 4603-4606; (b) Q. Lai, Q. Liu, Y. He, K. Zhao, C. Y. Wei, L. Wojtas, X. Shi and Z. Song, *Org. Biomol. Chem.*, 2018, **16**, 7801-7805.
- (a) P. Li, X. Wang, L. Liu, J. Lim, R. Zou and Y. Zhao, *J. Am. Chem. Soc.*, 2016, **138**, 2142-2145; (b) X. Guo, X. Feng, T. Han, S. Wang, Z. Lin, Y. Dong and B. Wang, *J. Am. Chem. Soc.*, 2014, **136**, 15485-15488; (c) P. Li, X. Wang and Y. Zhao, *Coord. Chem. Rev.*, 2019, **380**, 484-518; (d) V. Gupta and S. K. Mandal, *Chem. Euro. J.*, 2020, **26**, 2658-2665.
- S. Sengupta, H. Duan, W. Lu, J. L. Petersen and X. Shi, *Org. Lett.*, 2008, **10**, 1493-1496.
- J. Kalisiak, K. B. Sharpless and Valery V. Fokin, *Org. Lett.*, 2008, **10**, 3171-3174.
- (a) H. A. Lara-García, M. R. Gonzalez, J. H. González-Estefan, P. Sánchez-Camacho, E. Lima and I. A. Ibarra, *Inorg. Chem. Front.*, 2015, **2**, 442-447; (b) J. Canviet, A. Fateeva, Y. Guo, B. Coasne and D. Farrusseng, *Chem. Soc. Rev.*, 2014, **43**, 5594-5617.
- E. Sánchez-González, J. R. Álvarez, R. A. Peralta, A. Campos-Reales-Pineda, A. Tejada-Cruz, E. Lima, J. Balmaseda, E. González-Zamora and I. A. Ibarra, *ACS Omega*, 2016, **1**, 305-310.
- J. Li, R. J. Kuppler and H. Zhou, *Chem. Soc. Rev.*, 2009, **38**, 1477-1504.
- (a) R. Boulmène, M. Prakash and M. Hochlaf, *Phys. Chem. Chem. Phys.*, 2016, **18**, 29709-29720; (b) L.H. Xie and M. P. Suh, *Chem. Eur. J.*, 2013, **19**, 11590-1159.



73x40mm (600 x 600 DPI)